J. Earth Syst. Sci. (2023)132 135
https://doi.org/10.1007/s12040-023-02139-5

Vibrations analysis of propagation of SH-type wave influenced by a point source in a porous piezoelectric layered structure by Green's function approach

Neelima Bhengra[1], Raju Kumhar[2,*], Shishir Gupta[3] and Santimoy Kundu[3]

[1]*Department of Mathematics, Visvesvaraya National Institute of Technology, Nagpur 440 010, India.*
[2]*Department of Applied Sciences and Humanities, National Institute of Advanced Manufacturing Technology (NIFFT), Hatia, Ranchi 834 003, India.*
[3]*Department of Mathematics and Computing, Indian Institute of Technology (ISM), Dhanbad 826 004, India.*
**Corresponding author. e-mail: raju.ism92@gmail.com*

MS received 12 July 2021; revised 31 March 2023; accepted 3 May 2023

The principal objective of this paper is to investigate the propagation behaviour of SH-type waves incurred due to a point source in a porous piezoelectric layer resting over a heterogeneous viscoelastic substrate. The Green's function technique is used to determine the frequency equation which ultimately reduces to the classical Love wave equation as a special case of the present problem. Further, expressions for the particle displacement in the layer and substrate have been obtained. Some numerical computations and comparative analysis have been performed to demonstrate the behavioural characteristics of SH-type wave propagation under the influence of some of the critical factors such as heterogeneity parameter associated with rigidity, internal friction and, density. Other affecting factors include dissipation factor, attenuation coefficient, piezoelectric constant, the width of the PPM layer and dielectric constants, which have been unravelled and displayed graphically.

Keywords. Porous piezoelectric material; viscoelastic medium; dissipation factor; Green's function technique; attenuation coefficients; dielectric constant.

1. Introduction

In a world full of sophisticated mathematical techniques, Green's function technique stands out, given its practical applicability and its ability in determining the mathematical solutions to a large number of families of differential equations. It is very helpful in numerical and analytical techniques including singular integral equation methods, boundary element methods and dislocation methods. To be more precise, it creates visual interpretations of the operation associated to a point source. It is a known fact that the motions created in the material medium are not only caused due to internal disturbances but also due to external interactions. The external disturbing forces are functions of time and space. Therefore, there is one particular type of force that originate from unit impulsive force which can be defined with the help of Dirac's delta function. A class of elastodynamic problems involve such disturbances due to a point source which is a function of spatial coordinates and time. The Green's function plays a pivotal role in determining the mathematical solutions to these boundary value problems. Further, it has the ability to be defined according to the mechanical interactions occurring in the medium due to an impulsive excitation force. Many researchers have

Published online: 18 August 2023

their study on Green's function such as Covert (1958) established particle displacement for Love-type waves using Green's function. Followed by this, Ghosh (1963) studied the displacement of Love waves derived through a point source. Aki and Richards (1980) and Ben-Menahem and Singh (1981) have also made efforts to study Green's function extensively. Chattopadhyay *et al.* (2012) studied the effect of point source and heterogeneity on the propagation of SH waves in a viscoelastic layer over a viscoelastic half-space. In recent years, Singh *et al.* (2017, 2018), Karmakar *et al.* (2020), Kundu *et al.* (2020), Mahanty *et al.* (2021); and Kumari and Singh (2021) worked on point source as well as Green's function.

Piezoelectric crystals and ceramics exhibit distinctive electromechanical coupling characteristics which enable them to produce electrical fields under the application of mechanical loads and also display elastic deformation on applying electrical loads. Nowadays piezoelectric composite materials which consist of two or more piezoelectric materials have some drawbacks due to the failure of the mechanism under electrical or mechanical loading. The other limitation, higher acoustic impedance restricts the utilization of the device in under-sea application up to a certain depth in the field of earth science. The acoustic impedance is a significant prerequisite in designing sonar and other underwater object detection devices. Also, Love wave sensors in piezoelectric materials find applications in principal detectors, sensors, and actuators as well as in signal transmission. Generally, they are brittle in nature and attempts have often been made (Taunaumang *et al.* 1994; Chan *et al.* 1999) to develop composite piezoelectric structures to extenuate their brittleness and to reinforce the coupling effects between electrical and mechanical activities. Due to its brittleness and some other possible defects such as impurity, cavities, micro-voids, layer separations, inclusions and micro-cracks, the devices often have the tendency to fail. These problems can be mitigated by the introduction of controlled porosity into the piezoelectric material. The mismatching of impedance and failure rate of the piezoelectric composite device can be overcome altogether by taking the discrepancy in porosity of the piezoelectric material. Such porous piezoelectric materials (PPM) are extensively used in many applications such as miniature hydrophones, vibratory sensors, accelerometers and contact microphones. These PPMs with low acoustic impedance can improve the sensitivity of acoustic detectors by studying the propagation characteristics and localization behaviour of the wave at the surface of such piezoelectric configuration. Arai *et al.* (1991) studied the properties of hydrophones with porous piezoelectric ceramics. Hayashi *et al.* (1991) discussed the processing of Porous 3-3 PZT Ceramics using Capsule-Free O_2-HIP. Piezoelectric materials have one significant disadvantage, their low impedance value. Mizumura *et al.* (1991) studied the porous piezoelectric ceramic as transducer. The discussion talks about the low acoustic impedance of porous piezoelectric ceramics. To design efficient sonar devices, acoustic impedance is an essential requirement. The piezoelectric effect depends on a number of factors such as elastic constant, porosity, density and so on. Porosity variation can control the acoustic impedance remarkably and can reduce the issues such as device failure. Some recent works on this material have been mentioned below; Ezzin *et al.* (2016) studied the Love wave propagation in a transversely isotropic piezoelectric layer on a piezomagnetic half-space. Ezzin *et al.* (2017) discussed the propagation behaviour of SH waves in a layered piezoelectric/piezomagnetic plate. Singhal *et al.* (2018a, b) published a research paper on the approximation of surface wave frequency in piezocomposite structures. They also worked on Liouville–Green approximation: An analytical approach to study the elastic wave vibrations in the composite structure of piezo material. Ebrahimi and Barati (2017) did the vibration analysis of magneto-electro-elastic heterogeneous porous material plates resting on elastic foundation. Ebrahimi and Dabbagh (2017) also did the wave propagation analysis of smart rotating porous heterogeneous piezoelectric nanobeams. Ebrahimi *et al.* (2017) discussed the damping vibration analysis of smart piezoelectric polymeric nanoplates on viscoelastic substrate-based non-local strain gradient theory. Some other research works are: Nasedkin *et al.* (2017) did finite element simulation on effective properties of microporous piezoceramic material with metallized pore surfaces. Kudimova *et al.* (2017) emphasized the computer design of porous and ceramic piezocomposites in the finite element package. Sahu studied the Love-type waves in functionally graded piezoelectric material (FGPM) sandwiched between an initially stressed layer and elastic substrate. Some more eminent authors who have made their experimental studies that relate to porous piezoelectric materials are Xia *et al.* (2003), Paizza *et al.* (2005), Huang *et al.* (2006), Zeng *et al.* (2006), and Wang *et al.* (2008).

The present study delves into the propagation behaviour of SH-type wave originated from a point source in a porous piezoelectric material (PPM) layer lying over a heterogeneous viscoelastic substrate. Green's function technique has been effectively used to find the particle displacement of the SH-type wave. Significant efforts have been made to align the numerical calculations and graphical analysis with the assistance of two-dimensional plots. These plots contain variations of real phase velocity and damped velocity against real wave number with some of the affecting parameters such as heterogeneity parameter associated with rigidity, internal friction and density. Other factors include dissipation factor, attenuation coefficient, piezoelectric constant, width of the layer, dielectric coupling between two phases of the porous aggregate and dielectric constant. Eventually, they provide a visual analysis of the present paper for better interpretation. The outcomes provide a theoretical framework for designing and developing of underwater acoustic devices for sensing and non-destructive testing.

2. Mathematical formulation of the problem

Let us consider a porous piezoelectric material (PPM) layer of finite width H lying over a heterogeneous viscoelastic substrate. The y-axis is towards the direction of wave propagation, while the x-axis has been considered positive vertically downwards as shown in figure 1. The source of disturbance S has been taken at the point of intersection of the separation interface and x-axis. The polarization direction of porous piezoelectric material layer is parallel to z-axis and the material properties are assumed to be constant in the layer.

It is assumed that the displacement components for the PPM layer and heterogeneous viscoelastic substrate are given by $(u_{\text{ppm}}, v_{\text{ppm}}, w_{\text{ppm}})$ and (u_s, v_s, w_s), respectively. Therefore, for the propagation of SH-type wave in the y direction, it may be written that

$$u_{\text{ppm}} = 0, v_{\text{ppm}} = 0, w_{\text{ppm}} = w_{\text{ppm}}(x, y, t), u_s = 0, \\ v_s = 0, w_s = w_s(x, y, t), \partial_z \equiv 0. \tag{1}$$

2.1 *Dynamics of upper PPM layer under the influence of a point source*

The constitutive equations for porous piezoelectric medium are (Gupta and Venkatesh 2006)

$$\begin{aligned} \sigma_{ij} &= F_{ijkl}\varepsilon_{kl} + m_{ij}\varepsilon^* - e_{kij}E_k - \zeta_{kij}E_k^*, \\ \sigma^* &= m_{ij}\varepsilon_{ij} + R\varepsilon^* - \zeta_k E_k - e_k^* E_k^*, \\ D_i &= e_{ikl}\varepsilon_{kl} + \zeta_i\varepsilon^* + T_{il}E_l + A_{il}E_l^*, \\ D_i^* &= \zeta_{ikl}\varepsilon_{kl} + e_i^*\varepsilon^* + A_{il}E_l + T_{il}^*E_l^*, \end{aligned} \tag{2}$$

where $\sigma_{ij}(\sigma^*)$ and $\varepsilon_{ij}(\varepsilon^*)$ are the stress and strain tensor components for the solid (fluid) phase in the upper PPM layer, respectively. $D_i(D_i^*)$ and $E_i(E_i^*)$ are the electric displacement and electric field vector for the solid (fluid) phase in the upper PPM layer, respectively. Also F_{ijkl}, m_{ij}, R are elastic constants, $e_{ijk}, e_i^*, \zeta_{ijk}, \zeta_i$ are the piezoelectric constants, and T_{ij}, T_{ij}^*, A_{ij} are dielectric constants.

The equation of motion in the absence of body forces and surface charge density for PPM layer are as follows:

$$\begin{aligned} \sigma_{ij,j} &= (\rho_{11})_{ij}\ddot{u}_j + (\rho_{12})_{ij}\ddot{U}_j^* \\ \sigma_{,i}^* &= (\rho_{12})_{ij}\ddot{u}_j + (\rho_{22})_{ij}\ddot{U}_j^* \\ D_{i,i} &= 0, D_{i,i}^* = 0. \end{aligned} \tag{3}$$

Further, we have

$$\varepsilon_{ij} = \frac{1}{2}\left(u_{i,j} + u_{j,i}\right), \varepsilon^* = U_{i,i}^*, E_i = -\phi_{,i}, E_i^* = -\phi_{,i}^*. \tag{4}$$

Here u_i and U_i^* are the mechanical displacement components of PPM layer. $(\rho_{11})_{ij}$, $(\rho_{12})_{ij}$ and $(\rho_{22})_{ij}$ are dynamical mass coefficients. $\phi(\phi^*)$ is the electric potential function for the solid (fluid) phase for M_1.

If ρ_s is the mass density of solid part and ρ_l is the mass density of liquid part of the porous part, then we have the relation

$$\rho_{11} + \rho_{12} = (1 - f)\rho_s, \quad \rho_{11} + \rho_{12} = f\rho_l.$$

So that the total mass density is

$$\rho_1 = \rho_{11} + 2\rho_{12} + \rho_{22}.$$

Moreover, these mass coefficients obey the following inequalities

$$\rho_{11} > 0, \rho_{12} \leq 0, \rho_{22} > 0 \quad \text{and} \quad \rho_{11}\rho_{22} - \rho_{12}^2 > 0.$$

Also, $\gamma_{11} = \frac{\rho_{11}}{\rho_1}, \gamma_{12} = \frac{\rho_{12}}{\rho_1}$ and $\gamma_{22} = \frac{\rho_{22}}{\rho_1}$ are the non-dimensional material parameter of porous medium suggested by Karmakar *et al.* (2020).

Thus we conclude

- If the layer is non-porous solid, then $d \to 1$.
- If the layer is fluid, then $d \to 0$.

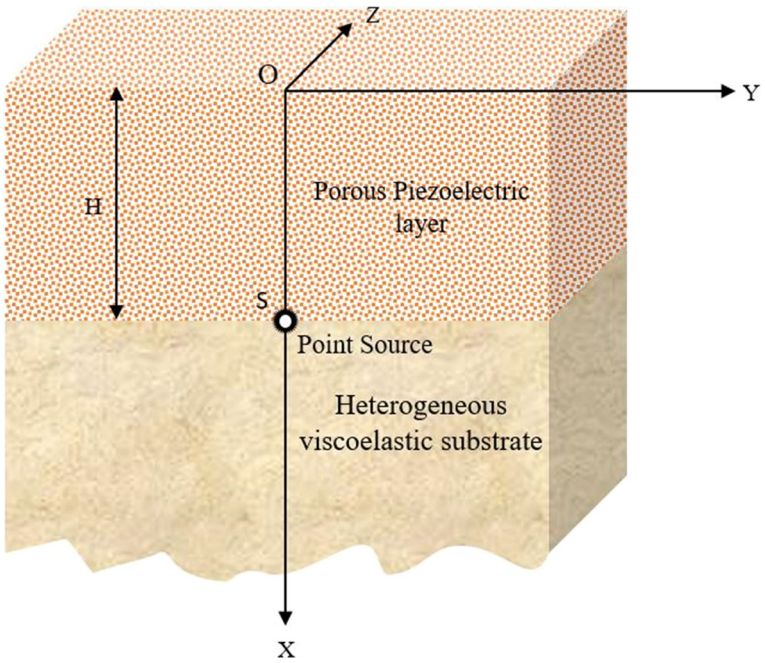

Figure 1. Schematic diagram of the problem.

- If the layer is poroelastic, then $0<d<1$,

where $d=\gamma_{11}-\frac{\gamma_{12}^2}{\gamma_{22}}$.

The constitutive equations for the PPM layer medium can be written as:

$$\sigma_{11}=F_{11}\varepsilon_{11}+F_{12}\varepsilon_{22}+F_{13}\varepsilon_{33}+m_{11}\varepsilon^*-e_{31}E_3$$

$$\sigma_{22}=F_{12}\varepsilon_{11}+F_{11}\varepsilon_{22}+F_{13}\varepsilon_{33}+m_{11}\varepsilon^*-e_{31}E_3$$

$$\sigma_{33}=F_{13}\varepsilon_{11}+F_{13}\varepsilon_{22}+F_{33}\varepsilon_{33}+m_{33}\varepsilon^*-e_{33}E_3$$

$$\sigma_{32}=2F_{44}\varepsilon_{32}-e_{15}E_2$$

$$\sigma_{31}=2F_{44}\varepsilon_{31}-e_{15}E_1$$

$$\sigma_{12}=2F_{66}\varepsilon_{12}$$

$$\sigma^*=m_{11}\varepsilon_{11}+m_{11}\varepsilon_{22}+m_{33}\varepsilon_{33}+R\varepsilon^*$$

$$D_1=2e_{15}\varepsilon_{13}+a_{11}E_1+A_{11}E_1^*$$

$$D_2=2e_{15}\varepsilon_{23}+a_{11}E_2+A_{11}E_2^*$$

$$D_3=e_{31}\varepsilon_{11}+e_{31}\varepsilon_{22}+e_{33}\varepsilon_{33}+\zeta_3\varepsilon^*+a_{33}E_3+A_{33}E_3^*$$

$$D_1^*=A_{11}E_1+a_{11}^*E_1^*$$

$$D_2^*=A_{11}E_2+a_{11}^*E_2^*$$

$$D_3^*=e_3^*\varepsilon^*+A_{33}E_3+a_{33}^*E_3^*. \tag{5}$$

where $F_{66}=\frac{(F_{11}-F_{12})}{2}$.

The constitutive relations and governing equations of transversely isotropic porous piezoelectric materials under anti-plane deformation are:

$$F_{44}\nabla^2 w_{\text{ppm}}+e_{15}\nabla^2\phi_{\text{ppm}}=\rho^p\ddot{w}_{\text{ppm}} \tag{6}$$

and

$$e_{15}\nabla^2 w_{\text{ppm}}-T_{11}^p\nabla^2\phi_{\text{ppm}}=0 \tag{7}$$

where

$$\nabla^2=\left(\partial_{xx}+\partial_{yy}\right),\rho^p=\rho_1\left(\gamma_{11}-\frac{(\gamma_{12})^2}{\gamma_{22}}\right)=\rho_1 d,$$

$$T_{11}^p=T_{11}-\frac{(A_{11})^2}{T_{11}^*},$$

and

$$\nabla^2\phi^*=-\frac{A_{11}}{T_{11}^*}\nabla^2\phi.$$

If the source is introduced in the form of Dirac-delta function, the expression for the displacement at a point on the surface is the same as the value of Green's function for the whole system at that point.

Let $\sigma_1(r,t)$ be considered as the force density distribution function for the upper layer due to the point source, then the equation of motion for SH-type wave propagating along the y-axis becomes:

$$F_{44}\nabla^2 w_{\text{ppm}} + e_{15}\nabla^2\phi_{\text{ppm}} - \rho^p \ddot{w}_{\text{ppm}} = 4\pi\sigma_1(r,t), \tag{8}$$

$$e_{15}\nabla^2 w_{\text{ppm}} - T_{11}^p\nabla^2\phi_m = 0 \tag{9}$$

where r is the distance from the origin at which the force was applied to a point and t is the time.

Now using the substitutions $w_{\text{ppm}}(x,y,t) = w_{\text{ppm}}(x,y)e^{i\omega t}$, $\phi_{\text{ppm}}(x,y,t) = \phi_{\text{ppm}}(x,y)e^{i\omega t}$ and $\sigma_1(r,t) = \sigma_1(r)e^{i\omega t}$ in the above equation, we obtain

$$F_{44}\nabla^2 w_{\text{ppm}} + e_{15}\nabla^2\phi_{\text{ppm}} + \rho^p\omega^2 w_{\text{ppm}} = 4\pi\sigma_1(r), \tag{10}$$

$$e_{15}\nabla^2 w_{\text{ppm}} - T_{11}^p\nabla^2\phi_{\text{ppm}} = 0 \tag{11}$$

where $\omega = kc$ is the angular frequency. Here, k and c are the wave number and phase velocity, respectively. Therefore, the disturbances caused by the impulsive force $\sigma_1(r)$ may be represented in terms of Dirac-delta function at the point source as $\sigma_1(r) = \delta(y)\delta(x-H)$.

Defining the Fourier transform $\overline{w}_{\text{ppm}}(\eta,x)$ of $w_{\text{ppm}}(x,y)$ as

$$\overline{w}_{\text{ppm}}(\eta,x) = \frac{1}{2\pi}\int_{-\infty}^{\infty} w_{\text{ppm}}(x,y)e^{i\eta y}dy \tag{12}$$

Then the inverse Fourier transform can be given as:

$$w_{\text{ppm}}(x,y) = \int_{-\infty}^{\infty} \overline{w}_{\text{ppm}}(\eta,x)e^{-i\eta y}d\eta \tag{13}$$

Now, applying the Fourier transform in equations (10 and 11), the following differential equations are obtained:

$$\begin{aligned} &F_{44}\left(D_{xx}\overline{w}_{\text{ppm}} - \eta^2\overline{w}_{\text{ppm}}\right) \\ &\quad + e_{15}\left(D_{xx}\overline{\phi}_{\text{ppm}} - \eta^2\overline{\phi}_{\text{ppm}}\right) + \rho^p\omega^2\overline{w}_{\text{ppm}} \\ &\quad = 2\delta(x-H), \end{aligned} \tag{14}$$

$$\begin{aligned} &e_{15}\left(D_{xx}\overline{w}_{\text{ppm}} - \eta^2\overline{w}_{\text{ppm}}\right) - T_{11}^p\left(D_{xx}\overline{\phi}_{\text{ppm}} - \eta^2\overline{\phi}_{\text{ppm}}\right) \\ &\quad = 0, \end{aligned} \tag{15}$$

Putting equation (15) in equation (14) yields

$$D_{xx}\overline{w}_{\text{ppm}} - \alpha^2\overline{w}_{\text{ppm}} = 4\pi\sigma_2(x) \tag{16}$$

where $\alpha^2 = \eta^2 - \frac{\rho^p\omega^2}{\overline{F}_{44}}$, $\sigma_2(x) = \frac{\delta(x-H)}{2\pi\overline{F}_{44}}$ and $\overline{F}_{44} = \left(F_{44} + \frac{e_{15}^2}{T_{11}^p}\right)$.

2.2 *Dynamics of lower heterogeneous viscoelastic substrate*

The stress–strain relations for homogeneous viscoelastic substrate are given by Borcherdt (2009)

$$\tau_{ij} = \overline{\lambda}\nabla\delta_{ij} + 2\overline{\mu}e_{ij}, \quad (i,j=1,2,3) \tag{17}$$

where $\overline{\mu} = \mu + \mu'\partial_t, \overline{\lambda} = \lambda + \lambda'\partial_t$.

The non-vanishing strain components e_{ij} in terms of displacement components may be obtained as:

$$e_{ij} = \frac{1}{2}\left(u_{i,j} + u_{j,i}\right). \tag{18}$$

Therefore, in light of equations (1, 18 and 17) give the components of stresses for the viscoelastic substrate are

$$\begin{aligned} &\tau_{11} = \left(\overline{\lambda} + 2\overline{\mu}\right)\partial_x u_s + \overline{\lambda}\partial_y v_s, \\ &\tau_{12} = \overline{\mu}\left(\partial_y u_s + \partial_y v_s\right), \tau_{13} = \overline{\mu}\partial_x w_s, \\ &\tau_{32} = \overline{\mu}\partial_y w_s. \end{aligned} \tag{19}$$

For the propagation of SH-type wave in y-direction, the only non-vanishing equation of motion can be written as:

$$\partial_x[(\mu + \mu'\partial_t)\partial_x w_s] + \partial_y\left[(\mu + \mu'\partial_t)\partial_y w_s\right] = \rho_2\ddot{w}_s. \tag{20}$$

Now, the heterogeneity of the lower heterogeneous viscoelastic substrate has been considered in the form

$$\begin{aligned} \mu &= \mu_0 + \chi_1(x-H)^n, \\ \mu' &= \mu_0' + \chi_2(x-H)^n, \\ \rho_2 &= \rho_2^0 + \chi_3(x-H)^n. \end{aligned} \tag{21}$$

where χ_1, χ_2 and χ_3 are small positive real constants having dimensions $\text{ML}^{-2}\text{T}^{-2}$, MT^{-1} and ML^{-4} are termed as frequency of inhomogeneity associated with rigidity, internal friction and density, respectively.

Therefore, substitution of equation (21) into equation (20) yields:

$$\begin{aligned} &\partial_x\left[\left(\mu_0 + \mu_0'\partial_t\right)\partial_x w_s + (x-H)^n(\chi_1 + \chi_2\partial_t)\partial_x w_s\right] \\ &\quad + \partial_y\left[\left(\mu_0 + \mu_0'\partial_t\right)\partial_y w_s + (x-H)^n(\chi_1 + \chi_2\partial_t)\partial_y w_s\right] \\ &\quad = \left[\rho_2^0 + \chi_3(x-H)^n\right]\ddot{w}_s. \end{aligned} \tag{22}$$

Now using the substitution $w_s(x,y,t) = w_s(x,y)e^{i\omega t}$ in the above equation, we get:

$$[\alpha_1 + \alpha_2(x-H)^n]\nabla^2 w_s + n(x-H)^{n-1}\alpha_2\partial_x w_s + \omega^2\left[\rho_2^0 + \chi_3(x-H)^n\right]w_s = 0. \quad (23)$$

where $\alpha_1 = \left(\mu_0 + i\omega\mu_0'\right)$ and $\alpha_2 = (\chi_1 + i\omega\chi_2)$.

Defining the Fourier transform $\overline{w}_s(\eta,x)$ of $w_s(x,y)$:

$$\overline{w}_s(\eta,x) = \frac{1}{2\pi}\int_{-\infty}^{\infty} w_s(x,y)e^{i\eta y}dy. \quad (24)$$

Then the inverse transform can be given as:

$$w_s(x,y) = \int_{-\infty}^{\infty} \overline{w}_s(\eta,x)e^{-i\eta y}d\eta. \quad (25)$$

Using Fourier transformation in equation (23), we have

$$D_{xx}\overline{w}_s - \beta^2\overline{w}_s = 4\pi\sigma_3(x) \quad (26)$$

where

$$\beta^2 = \frac{\left[\alpha_1\eta^2 - \rho_2^0\omega^2\right]}{\alpha_1},$$

$$4\pi\sigma_3(x) = -1/\alpha_1\Big[\alpha_2(x-H)^n D_{xx}\overline{w}_s + n(x-H)^{n-1} \times\alpha_2 D_x\overline{w}_s - (x-H)^n\left\{\alpha_2\eta^2 - \chi_3\omega^2\right\}\overline{w}_s\Big].$$

2.3 *Boundary conditions*

Some of the boundary conditions that need to be satisfied by the geometry of the problem are as follows:

a) The uppermost surface must be free from shear stress, electrical displacement and electrical potential function at the interface $x = 0$.

$$\sigma_{13} = 0. \quad (27)$$

$$\overline{\phi}_{\text{ppm}}(x,y) = 0. \quad (28)$$

$$D_x(x,y) + D_x^*(x,y) = 0. \quad (29)$$

b) The periodicity of the components of the stress, mechanical displacement and electrical potential function at $x = H$ leads to the following conditions:

$$\sigma_{13} = \tau_{13}. \quad (30)$$

$$\overline{w}_{\text{ppm}}(x,y) = \overline{w}_s(x,y). \quad (31)$$

$$\overline{\phi}_{\text{ppm}}(x,y) = 0. \quad (32)$$

Now, to deduce the expression for displacements in the layer as well as in the substrate, boundary conditions equation (27) with equation (29) and equation (30) with equation (32) are combined to obtain

$$D_x\overline{w}_{\text{ppm}} = 0, \text{ at } x = 0 \quad (33)$$

and

$$F_{44}D_x\overline{w}_{\text{ppm}} = \alpha_1 D_x\overline{w}_s, \text{ at } x = H. \quad (34)$$

respectively.

Now, let $G_{\text{ppm}}(x/x_0)$ be the Green's function for the PPM layer satisfying the condition $D_x G_{\text{ppm}} = 0$ at $x = 0, H$ and x_0 is an arbitrary point in the medium, then the equation satisfied by $G_{\text{ppm}}(x/x_0)$ is

$$D_{xx}G_{\text{ppm}}(x/x_0) - \alpha^2 G_{\text{ppm}}(x/x_0) = \delta(x-x_0) \quad (35)$$

$G_{\text{ppm}}(x/x_0)$ and $\overline{w}_{\text{ppm}}$ when multiplied with equations (16) and (35), respectively and then resulting equations subtracted and further integrated with respect to x from $x = 0$ to H yield

$$\int_{x=0}^{H}\left[G_{\text{ppm}}(x/x_0)D_{xx}\overline{w}_{\text{ppm}} - \overline{w}_{\text{ppm}}(x/x_0)D_{xx}G_{\text{ppm}}\right]dx = \int_{x=0}^{H} 4\pi\sigma_2(x)G_{\text{ppm}}(x/x_0)dx - \int_{x=0}^{H}\delta(x-x_0)\overline{w}_{\text{ppm}}dx \quad (36)$$

with the help of the conditions $D_x G_{\text{ppm}}(x/x_0) = 0$ at $x = 0$ and H, equation (36) results in

$$G_{\text{ppm}}(H/x_0)\left[D_x\overline{w}_{\text{ppm}}\right]_{x=H} = \frac{2}{\overline{F}_{44}}G_{\text{ppm}}(H/x_0) - \overline{w}_{\text{ppm}}(x_0). \quad (37)$$

Thus, the expression for displacement in the PPM layer $\overline{w}_{\text{ppm}}$ at any point, x is obtained as

$$\overline{w}_{\text{ppm}}(x) = \frac{2}{\overline{F}_{44}}G_{\text{ppm}}(x/H) - G_{\text{ppm}}(H/x)\left[D_x\overline{w}_{\text{ppm}}\right]_{x=H} \quad (38)$$

where x_0 is replaced by x and noting that $G_{\text{ppm}}(H/x) = G_{\text{ppm}}(x/H)$.

Let $G_s(x/x_0)$ be the Green's function for the substrate satisfying the condition $D_x G_s = 0$ at $x = H$ and it also approaches zero as x tends to infinity.

The equation which is satisfied by $G_s(x/x_0)$ may be written as:

$$D_{xx} G_s(x/x_0) - \beta^2 G_s(x/x_0) = \delta(x - x_0) \tag{39}$$

$G_s(x/x_0)$ and $\overline{w}_s$ when multiplied to equations (26 and 39), respectively and then resulting equations are subtracted and further integrated with respect to x from $x = H$ to ∞ yield

$$\begin{aligned}\int_{x=H}^{\infty} &[G_s(x/x_0) D_{xx}\overline{w}_s - \overline{w}_s(x/x_0) D_{xx} G_s] dx \\ &= \int_{x=H}^{\infty} 4\pi\sigma_3(x) G_s(x/x_0)\, dx \\ &- \int_{x=H}^{\infty} \delta(x - x_0)\overline{w}_s\, dx. \end{aligned} \tag{40}$$

Replacing x_0 by x in equation (40), and keeping in mind that $G_s(H/x) = G_s(x/H)$ and $G_s(x/x_0) = G_s(x_0/x)$, the expression for displacement $\overline{w}_s(x)$ at any point x in substrate is obtained as:

$$\begin{aligned}\overline{w}_s(x) = G_s(x/H)[D_x\overline{w}_s]_{x=H} \\ + \int_{x=H}^{\infty} 4\pi\sigma_3(x_0) G_s(x/x_0)\, dx_0. \end{aligned} \tag{41}$$

With the help of equation (34), the above equation gives

$$\begin{aligned}\left[D_x\overline{w}_{\text{ppm}}\right]_{x=H} = &\frac{\left(2/\overline{F}_{44}\right) G_{\text{ppm}}(H/H)}{(F_{44}/\alpha_1) G_s(H/H) + G_{\text{ppm}}(H/H)} \\ &- \frac{\int_{x=H}^{\infty} 4\pi\sigma_3(x_0) G_s(H/x_0)\, dx_0}{(F_{44}/\alpha_1) G_s(H/H) + G_{\text{ppm}}(H/H)}. \end{aligned} \tag{42}$$

Substituting the value of $\left[D_x\overline{w}_{\text{ppm}}\right]_{x=H}$ from equation (42) into equation (38), we obtain

$$\begin{aligned}\overline{w}_{\text{ppm}} = &\frac{\frac{2F_{44}}{\overline{F}_{44}} G_{\text{ppm}}(x/H) G_s(H/H)}{\left\{F_{44} G_s(H/H) + \alpha_1 G_{\text{ppm}}(H/H)\right\}} \\ &- \frac{G_{\text{ppm}}(x/H) \int_{x=H}^{\infty} 4\pi\sigma_3(x_0) G_s(H/x_0)\, dx_0}{\frac{1}{\alpha_1}\left\{F_{44} G_s(H/H) + \alpha_1 G_{\text{ppm}}(H/H)\right\}}. \end{aligned} \tag{43}$$

Moreover, employing the expression of $4\pi\sigma_3(x_0)$, the equation (43) may be rewritten as:

$$\begin{aligned}\bar{w}_{\text{ppm}} = &\frac{\frac{2F_{44}}{\overline{F}_{44}} G_{\text{ppm}}(x/H) G_s(H/H)}{\left\{F_{44} G_s(H/H) + \alpha_1 G_{\text{ppm}}(H/H)\right\}} \\ &- \frac{G_{\text{ppm}}(x/H)}{\left\{F_{44} G_s(H/H) + \alpha_1 G_m(H/H)\right\}} \\ &\times \int_{x=H}^{\infty} [\alpha_2 (x_0 - H)^n D_{x_0 x_0}\bar{w}_s \\ &+ n(x_0 - H)^{n-1} D_{x_0}\bar{w}_s \\ &- (x_0 - H)^n \left\{\alpha_2\eta^2 - \chi_3\omega^2\right\}\bar{w}_s] G_s(H/x_0)\, dx_0. \end{aligned} \tag{44}$$

Again using equations (34 and 41) and proceeding as mentioned previously, the value of $\overline{w}_s$ is obtained as:

$$\begin{aligned}\bar{w}_s = &\frac{\frac{2F_{44}}{\overline{F}_{44}} G_{\text{ppm}}(H/H) G_s(x/H)}{\left\{F_{44} G_s(H/H) + \alpha_1 G_{\text{ppm}}(H/H)\right\}} \\ &+ \frac{(F_{44}) G_s(x/H)}{\left\{F_{44} G_s(H/H) + \alpha_1 G_{\text{ppm}}(H/H)\right\}} \\ &\times \int_{H}^{\infty} [\alpha_2 (x_0 - H)^n D_{x_0 x_0}\bar{w}_s \\ &+ n(x_0 - H)^{n-1}\alpha_2 D_{x_0} - (x_0 - H)^n \\ &\times \left\{\alpha_2\eta^2 - \chi_3\omega^2\right\}\bar{w}_s] G_s(H/x_0)\, dx_0 - (1/\alpha_1) \\ &\times \int_{H}^{\infty} \left[\alpha_2 (x_0 - H)^n D_{x_0 x_0}\bar{w}_s + n(x_0 - H)^{n-1}\alpha_2 D_{x_0}\bar{w}_s \right. \\ &\left. - (x_0 - H)^n \left\{\alpha_2\eta^2 - \chi_3\omega^2\right\}\bar{w}_s\right] G_s(H/x_0)\, dx_0. \end{aligned} \tag{45}$$

Neglecting the higher powers of χ_1, χ_2 and χ_3, the expression for displacement in the heterogeneous viscoelastic substrate, as the first-order approximation is

$$\overline{w}_s(x) = \frac{\frac{2F_{44}}{\overline{F}_{44}} G_{\text{ppm}}(H/H) G_s(x/H)}{\left\{F_{44} G_s(H/H) + \alpha_1 G_{\text{ppm}}(H/H)\right\}} \tag{46}$$

which gives the displacement at any point in the heterogeneous viscoelastic substrate, if it is taken as homogeneous, putting this value of $\overline{w}_s(x)$ in equation (44), we get:

$$\bar{w}_{\text{ppm}} = \frac{\frac{2F_{44}}{\bar{F}_{44}} G_{\text{ppm}}(x/H) G_s(H/H)}{\{F_{44} G_s(H/H) + \alpha_1 G_{\text{ppm}}(H/H)\}} - \frac{(2F_{44}/\bar{F}_{44}) G_{\text{ppm}}(x/H) G_{\text{ppm}}(H/H)}{\{F_{44} G_s(H/H) + \alpha_1 G_{\text{ppm}}(H/H)\}^2} \times \int_H^\infty [(x_0 - H)^n \alpha_2 D_{x_0 x_0} G_s(x_0/H) + n(x_0 - H)^{n-1} \alpha_2 D_{x_0} G_s(x_0/H) - (x_0 - H)^n \{\alpha_2 \eta^2 - \chi_3 \omega^2\} \times G_s(x_0/H)] G_s(H/x_0) dx_0. \quad (47)$$

The solution of equation (47) represents the elastic displacements due to a unit impulsive force in space and time.

To evaluate $\overline{w}_{\text{ppm}}$, the values of $G_{\text{ppm}}(x/H)$ is required and must be determined.

Now, in order to obtain the solution of equation (16), which is satisfied by $G_{\text{ppm}}(x/x_0)$, let the two independent solutions of the equation

$$D_{xx} Q - \alpha^2 Q = 0, \quad (48)$$

vanishing at $x = -\infty$ and $x = \infty$ be $Q_1(x) = e^{\alpha x}$ and $Q_2(x) = e^{-\alpha x}$.

Therefore, the solution of equation (48) for an infinite medium is $-\frac{e^{-\alpha|x-x_0|}}{2\alpha}$.

$G_{\text{ppm}}(x/x_0)$ should satisfy the equation $D_x G_{\text{ppm}}(x/x_0) = 0$ at both $x = 0$ and H, it may be written as:

$$G_{\text{ppm}}(x/x_0) = -\frac{e^{-\alpha|x-x_0|}}{2\alpha} + Ae^{\alpha x} + Be^{-\alpha x} \quad (49)$$

where A and B are arbitrary constants. With the help of the aforementioned stated conditions, $G_{\text{ppm}}(x/x_0)$ is obtained as

$$G_{\text{ppm}}\left(\frac{x}{x_0}\right) = \frac{-1}{2\alpha}\left[e^{-\alpha|x-x_0|} + \frac{e^{\alpha x}\left(e^{\alpha|x-x_0|} + e^{-\alpha|x-x_0|}\right)}{e^{\alpha x} - e^{-\alpha x}} + \frac{e^{-\alpha x}\left(e^{\alpha|x-x_0|} + e^{-\alpha|x-x_0|}\right)}{e^{\alpha x} - e^{-\alpha x}}\right]. \quad (50)$$

Proceeding in a similar way and given equation (26), $G_s(x/x_0)$ may be obtained as:

$$G_s(x/x_0) = \frac{-1}{2\beta}\left[e^{-\beta|x-x_0|} + e^{-\beta|x+x_0-2H|}\right]. \quad (51)$$

Moreover, the following values for further usage may be easily derived from equations (49, 50 and 51):

$$G_{\text{ppm}}(x/H) = -\frac{e^{\alpha x} + e^{-\alpha x}}{\alpha(e^{\alpha H} - e^{-\alpha H})}, \quad (52)$$

$$G_{\text{ppm}}(H/H) = -\frac{e^{\alpha H} + e^{-\alpha H}}{\alpha(e^{\alpha H} - e^{-\alpha H})}, \quad (53)$$

$$G_s(H/x_0) = -\frac{e^{\alpha(x_0 - H)}}{\beta}, \quad (54)$$

$$G_s(H/H) = -\frac{1}{\beta}. \quad (55)$$

3. Frequency equation

Substitution of the values from equations (52, 53, 54 and 55) in equation (47) leads to

$$\overline{w}_{\text{ppm}}(x) = -\frac{2F_{44}}{\overline{F}_{44}} \times \frac{(e^{\alpha x} + e^{-\alpha x})}{\eta_3 - \eta_4}\left[1 + \frac{(e^{\alpha H} + e^{-\alpha H})}{\eta_3 - \eta_4}\chi_4\right] \quad (56)$$

where

$$\eta_3 = e^{\alpha H}(\alpha F_{44} + \beta\alpha_1), \quad \eta_4 = e^{-\alpha H}(\alpha F_{44} - \beta\alpha_1)$$

and

$$\chi_4 = \frac{\Gamma(n+1)}{2^{n+1}\beta^{n+1}}\left[-\alpha_2 - \frac{1}{\beta^2}\{\alpha_2\eta^2 - \chi_3\omega^2\}\right].$$

Equation (56) is further simplified to yield

$$\overline{w}_{\text{ppm}}(\eta, x) = \frac{-\frac{2F_{44}}{\overline{F}_{44}}(e^{\alpha x} + e^{-\alpha x})}{(\eta_3 - \eta_4) - (e^{\alpha H} + e^{-\alpha H})\chi_4}. \quad (57)$$

Taking the inverse Fourier transform of $\overline{w}_{\text{ppm}}$ in equation (57), the displacement in the PPM layer may be obtained as:

$$w_{\text{ppm}}(x, y) = \int_{-\infty}^{\infty} \frac{-\frac{2F_{44}}{\overline{F}_{44}}(e^{\alpha x} + e^{-\alpha x})e^{-i\eta y} d\eta}{(\eta_3 - \eta_4) - \chi_4(e^{\alpha H} + e^{-\alpha H})}. \quad (58)$$

The frequency equation of SH-type waves will be obtained by equating to zero the denominator of the above integral, i.e.,

$$e^{\alpha H}(\alpha F_{44} + \beta\alpha_1) - e^{-\alpha H}(\alpha F_{44} - \beta\alpha_1) - (e^{\alpha H} + e^{-\alpha H}) \times \frac{\Gamma(n+1)}{2^{n+1}\beta^{n+1}} \times \left[-\alpha_2 - \frac{1}{\beta^2}\{\alpha_2\eta^2 - \chi_3\omega^2\}\right] = 0. \quad (59)$$

Replacing η by k, ω by kc and α by $i\alpha_0$, then the closed form of velocity (equation 59) is obtained as:

$$\tan\alpha_0 H = \frac{\beta\alpha_1}{\alpha_0 F_{44}} - \frac{1}{\alpha_0 F_{44}} \times \left[\frac{\Gamma(n+1)}{2^{n+1}\beta^{n+1}}\left[-\alpha_2 - \frac{1}{\beta^2}\left\{\alpha_2\eta^2 - \chi_3\omega^2\right\}\right]\right] \quad (60)$$

where

$$\alpha_1 = \left(\mu_0 + ikc\mu_0'\right),$$

$$\alpha_2 = \left(\gamma_1 + ikc\gamma_2\right),$$

$$\alpha_0^2 = \frac{\rho^p k^2 c^2}{\overline{F}_{44}} - k^2$$

and

$$\beta^2 = \frac{\left[\alpha_1 k^2 - \rho_2^0 (kc)^2\right]}{\alpha_1}.$$

Equation (60) is the shear wave period equation for porous piezoelectric layer lying over a heterogeneous viscoelastic substrate due to the point source S.

Let the complex wave number k be expressed by:

$$k = k_1 + ik_2 = k_1(1 + i\delta) \quad (61)$$

where $\delta = \frac{k_2}{k_1}$ is the attenuation coefficient. The dimensionless dissipation factor is given by

$$Q_0^{-1} = \frac{\mu_0'\omega^*}{\mu_0} \quad (62)$$

where $\omega^* = \mathrm{Re}(k)c$. Equation (60) is complex due to the presence of dissipation, attenuation and complex wave number, thus on separating equation (60) into real and imaginary parts yields two real non-linear equations

$$\mathrm{Re}[\gamma_n(k,c)] = 0, \quad (63)$$

$$\mathrm{Im}[\gamma_n(k,c)] = 0. \quad (64)$$

Equation (63) is the frequency equation of SH-type wave propagation due to a disturbing source point which originates the dispersion curve, i.e., phase velocity against real wave number; equation (64) is the damping equation of SH-type waves which produces the damping characteristics of a wave.

After simplification of equations (63 and 64), we get:

$$\mathrm{Re}[\gamma_n(k,c)] = \frac{\sin 2t_1}{\cos 2t_1 + \cosh 2t_2} = \frac{q_1 q_3 + q_2 q_4}{q_3^2 + q_4^2} \quad (65)$$

$$\mathrm{Im}[\gamma_n(k,c)] = \frac{\sinh 2t_2}{\cos 2t_1 + \cosh 2t_2} = \frac{q_2 q_3 - q_1 q_4}{q_3^2 + q_4^2} \quad (66)$$

where q_1, q_2, q_3 and q_4 are given in Appendix A.

So far, only the displacements of the layer and substrate have been taken into consideration. Now, the purpose is to find the expression for scalar potential $\phi(x)$ equation (11) suggests that the special solution of it is given by:

$$\phi_{\mathrm{ppm}}^{(s)} = \frac{e_{15}}{T_{11}^p} w_{\mathrm{ppm}}, \quad (67)$$

and solution of homogeneous equation corresponding to equation (16) is given as:

$$\phi_{\mathrm{ppm}}^{(h)} = Ce^{-\eta x} + De^{\eta x} \quad (68)$$

where C and D are arbitrary constants, 's' and 'h' are superscripts and correspond to special and homogeneous solution, respectively. Therefore, combining equations (67 and 68), the complete solution of $\overline{\phi}(x)$ may be written as:

$$\overline{\phi}_{\mathrm{ppm}}(x) = Ce^{-\eta x} + De^{\eta x} + \frac{e_{15}}{T_{11}^p}\overline{w}_{\mathrm{ppm}}. \quad (69)$$

In light of boundary conditions equations (28, 32 and 15), equation (69) results in

$$\phi_{\mathrm{ppm}}(x,y) = \int_{-\infty}^{\infty} \frac{\frac{2c_{44}^m h_{15}}{\overline{c}_{44}^m \mu_{11}}\left[\left(e^{\eta(H-y)} + e^{-\eta(H-y)}\right) - \left(e^{\eta y} + e^{-\eta y}\right)\left(e^{\alpha H} + e^{-\alpha H}\right) - \left(e^{\alpha y} + e^{-\alpha y}\right)\left(e^{\eta H} + e^{-\eta H}\right)\right]}{(\eta_3 - \eta_4) - \chi(e^{\alpha H} + e^{-\alpha H})\left\{\frac{1}{2\beta} + \frac{\left[4\beta^3 - \omega^2 + \frac{3}{2}\eta^2\right]}{4\beta^3}\right\}} \times e^{-i\eta y} d\eta. \quad (70)$$

On solving the integrand appearing in equation (70) for poles, we arrive at equation (59) which is the frequency equation of SH-type wave propagating in a PPM layer under the influence of a point source and lying over a heterogeneous viscoelastic substrate.

4. Special cases

Case 1: When porous piezoelectric material becomes non-piezoelectric porous material, i.e., $e_{15} = T_{11} = T_{11}^{*} = A_{11} = 0$, then we have:

$$\mathrm{Re}[\gamma_n(k,c)] = \frac{\sin 2t_1}{\cos 2t_1 + \cosh 2t_2} = \frac{q_{11}q_{13} + q_{12}q_{14}}{q_{13}^2 + q_{14}^2} \tag{71}$$

$$\mathrm{Im}[\gamma_n(k,c)] = \frac{\sinh 2t_2}{\cos 2t_1 + \cosh 2t_2} = \frac{q_{12}q_{13} - q_{11}q_{14}}{q_{13}^2 + q_{14}^2} \tag{72}$$

where q_{11}, q_{12}, q_{13} and q_{14} are given in Appendix B.

Equation (71) is the frequency equation for SH-type wave propagation in a non-piezoelectric layer lying over a heterogeneous viscoelastic substrate. Equation (72) is the damping equation for SH-type wave propagation in a non-piezoelectric layer lying over a heterogeneous viscoelastic substrate.

Case 2: When porous piezoelectric material becomes isotropic material, i.e., $e_{15} = T_{11} = T_{11}^{*} = A_{11} = 0, F_{44} = \mu_1$ and $d \to 1$ and lower heterogeneous viscoelastic medium become isotropic, i.e., $\delta = 0, Q_0^{-1} = 0, \chi_1 = 0, \chi_2 = 0$ and $\chi_3 = 0$, then we have:

$$\tan kH\left[\frac{c^2}{c_1^2} - 1\right]^{\frac{1}{2}} = \frac{\mu_0\left[1 - \frac{c^2}{c_2^2}\right]^{\frac{1}{2}}}{\mu_1\left[\frac{c^2}{c_1^2} - 1\right]^{\frac{1}{2}}} \tag{73}$$

where

$$c_1 = \sqrt{\frac{\mu_1}{\rho_1}} \quad \text{and} \quad c_2 = \sqrt{\frac{\mu_0}{\rho_2^0}}.$$

Equation (73) is the well-known frequency equation given by Ewing *et al.* (1957), Qian *et al.* (2010) and Kumari *et al.* (2016) for Love wave propagation in an isotropic layer lying over an isotropic half-space which validates the current problem.

5. Numerical calculation and discussion

With a view to give better perception of the present study, i.e., the analysis of propagation of SH-type wave in PPM layer resting over a heterogeneous viscoelastic substrate, the authors have endeavoured with the help of two-dimensional plots. These plots refer to the variation of phase and damped velocities drawn against real wave number ($\mathrm{Re}[k_1 H]$) under the influence of parameters such as heterogeneity parameter associated with rigidity $\left(\Pi_1 = \frac{\chi_1 H^n}{\mu_0}\right)$, internal friction $\left(\Pi_2 = \frac{\chi_2 H^n}{\mu_0'}\right)$ and density $\left(\Pi_3 = \frac{\chi_3 H^n}{\rho_0}\right)$. Other plots include variation of phase and damped velocities against real wave number under the influence of dissipation factor (Q_0^{-1}), attenuation coefficient (δ), piezoelectric constant (e_{15}), width of the PPM layer (H) and dielectric constants (A_{11} and T_{11}).

For calculation purposes, we have taken some elastic constants of one of the porous piezoelectric materials (PZT-5H), which are given in table 1.

Additionally, some other data that have been used for viscoelastic substrate are from Gubbins (1990)

$$\mu_0 = 7.1 \times 10^{10}\ \mathrm{N/m^2},$$

$$\rho_0 = 3321\ \mathrm{kg/m^3}$$

$$\mu_0/\mu_0' = 30\ \mathrm{s^{-1}}.$$

Figures 2 and 3 represent the variation of real phase velocity and damped velocity against real wave number, respectively under the influence of heterogeneity parameter associated with rigidity $\left(\Pi_1 = \frac{\chi_1 H^n}{\mu_0}\right)$. It is observed that the phase velocity has an increasing behaviour under the influence of the considered parameter. While on the other hand, the damped velocity has a decreasing effect. The effect of Π_1 on damped velocity is more for smaller values of wave number and as the wave number increases this effect decreases gradually until it becomes almost negligible.

Figures 4 and 5 have been plotted to demonstrate the effect of heterogeneity parameter associated with internal friction $\left(\Pi_2 = \frac{\chi_2 H^n}{\mu_0'}\right)$ on phase and damped velocities, respectively. Both the phase and damped velocities exhibit mixed characteristics under the influence of Π_2, i.e., initially,

Table 1. *Elastic constants for porous piezoelectric material (Gupta and Venkatesh 2006).*

Material	Elastic constants ($\times 10^{10}$ N/m^2)	Piezoelectric constant (C/m^2)	Dielectric constants (10^{-10} F/m)	Mass density (kg/m^3)
PZT-5H	$C_{44} = 2.3$	$e_{15} = 17$	$T_{11} = 277$ $T^*_{11} = 299$ $A_{11} = 112$	$(\rho_{11})_{33} = 4950$ $(\rho_{12})_{33} = -1125$ $(\rho_{22})_{33} = 4800$

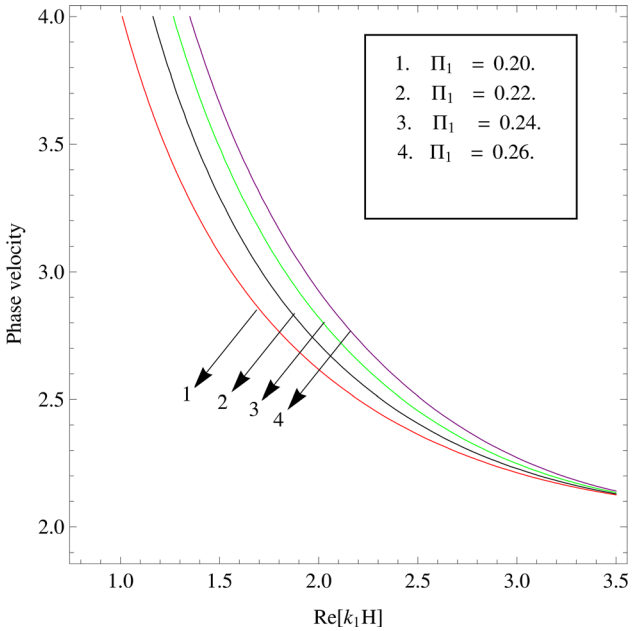

Figure 2. Variation of phase velocity against real wave number for different values of heterogeneity parameter associated with rigidity ($\Pi_1 = \frac{\chi_1 H^n}{\mu_0}$).

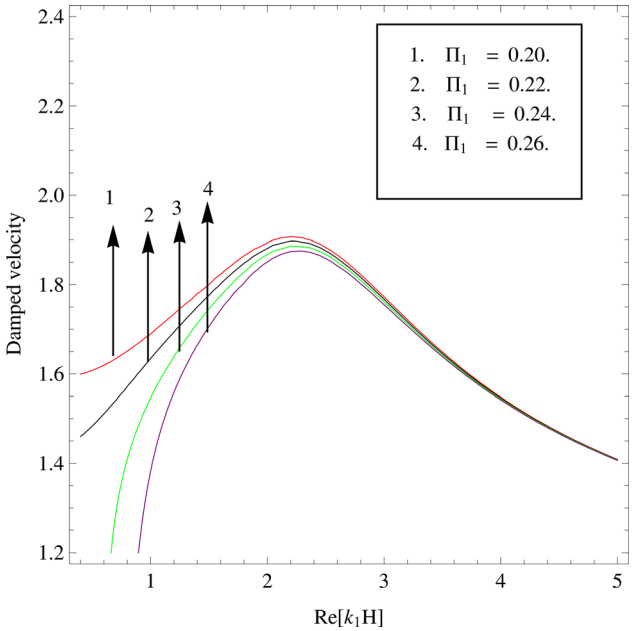

Figure 3. Variation of damped velocity against real wave number for different values of heterogeneity parameter associated with rigidity ($\Pi_1 = \frac{\chi_1 H^n}{\mu_0}$).

they get decreased but after some point, the behaviour changes and the velocities are increased.

Figures 6 and 7 portray the effect of heterogeneity parameter associated with density $\left(\Pi_3 = \frac{\chi_3 H^n}{\rho_0}\right)$. This parameter puts a constant increasing effect on the phase velocity while the damped velocity undergoes variable behaviour. However, looking at the curves it can be said that Π_3 puts positive influence on the damped velocity as well.

The effect of dissipation factor (Q_0^{-1}) on the phase velocity and the damped velocity have been discussed in figures 8 and 9. Looking carefully at the curves, it is observed that the dissipation factor has a favourable influence on the phase velocity. On the other hand, the effect on damped velocity is more noticeable in the higher frequency region. Here as well, Q_0^{-1} exerts a positive effect on the damped velocity.

The influence of attenuation coefficient (δ) on the phase and damped velocities have been presented in figures 10 and 11. It reveals that δ puts an unfavourable influence on the phase velocity. This effect is constant throughout. While in figure 11, it is observed that δ exerts a negative influence on the damped velocity as well. Here, the effect is more pronounced for smaller values of real wave number.

Figures 12 and 13 depict the variation of phase and damped velocities under the influence of piezoelectric constant (e_{15}). Observing the curves, the phase velocity has an increasing characteristic with e_{15} constantly, irrespective of the real wave number. While on the other curve, the damped velocity has a slight decrement with piezoelectric

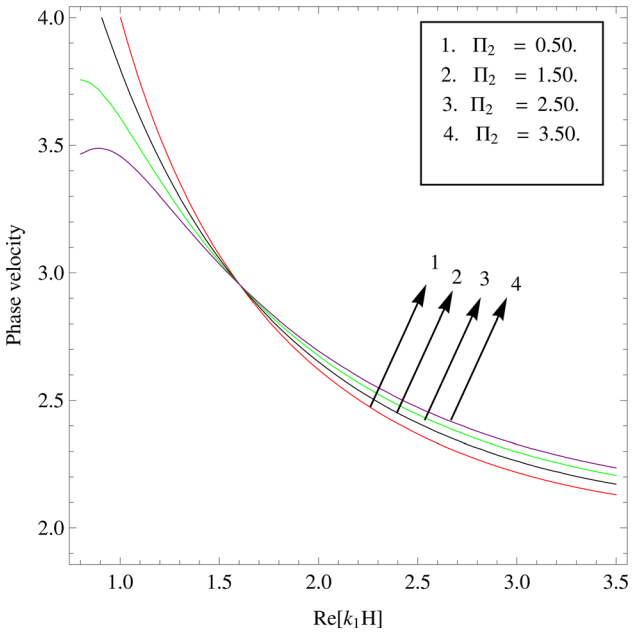

Figure 4. Variation of phase velocity against real wave number for different values of heterogeneity parameter associated with internal friction ($\Pi_2 = \frac{\zeta_2 H^n}{\mu_0'}$).

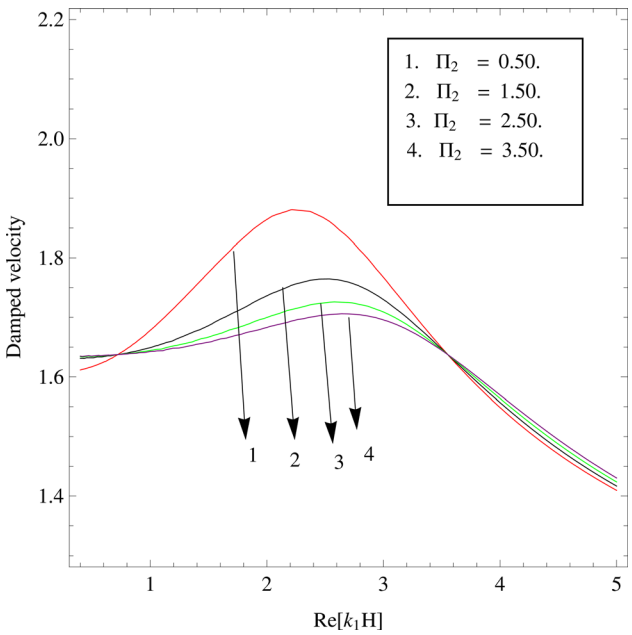

Figure 5. Variation of damped velocity against real wave number for different values of heterogeneity parameter associated with internal friction ($\Pi_2 = \frac{\zeta_2 H^n}{\mu_0'}$).

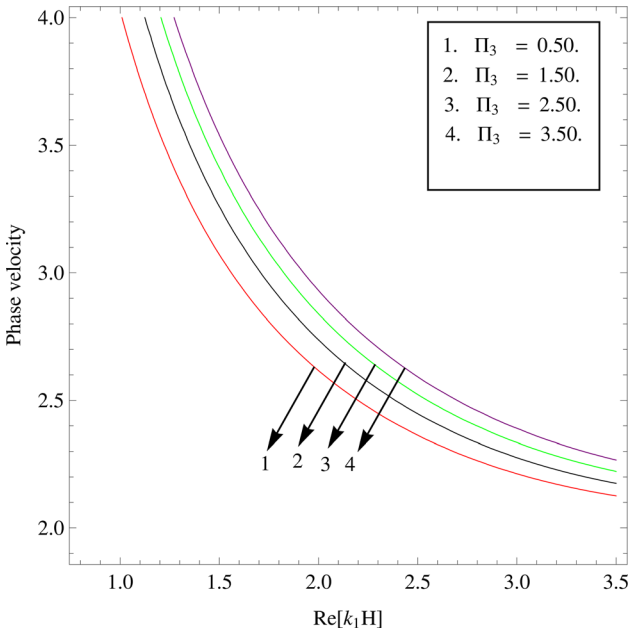

Figure 6. Variation of phase velocity against real wave number for different values of heterogeneity parameter associated with density ($\Pi_3 = \frac{\zeta_3 H^n}{\rho_2^0}$).

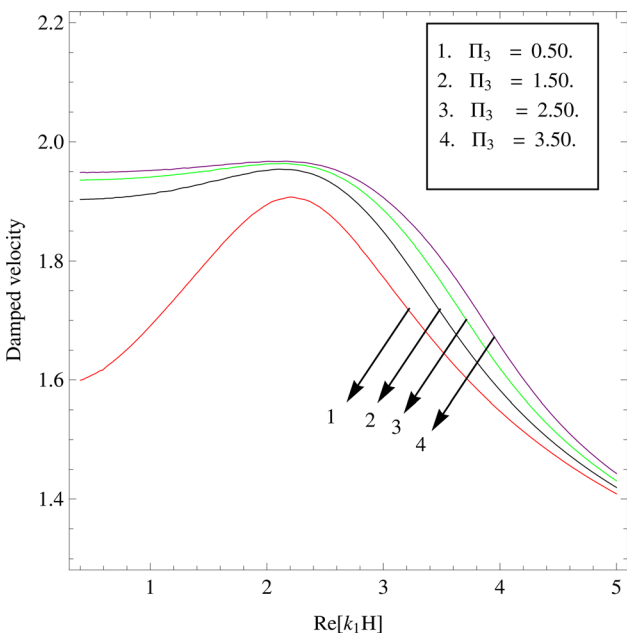

Figure 7. Variation of damped velocity against real wave number for different values of heterogeneity parameter associated with density ($\Pi_3 = \frac{\zeta_3 H^n}{\rho_2^0}$).

constant in the low-frequency region. At the high-frequency region, e_{15} puts a positive influence on the damped velocity.

The purpose of figures 14 and 15 is to demonstrate the influence of different values of the width of the PPM layer (H). The variation of phase and damped velocities are very similar to the variation discussed due to e_{15}.

Figures 16 and 17 exhibit the variation of phase and damped velocities under the influence of dielectric constant (A_{11}). The phase, as well as damped velocity, have negligible effects due to A_{11}. However, the phase velocity decreases gradually with wave number. While damped velocity has a slight increase initially which then forms a peak and afterwards it decreases gradually.

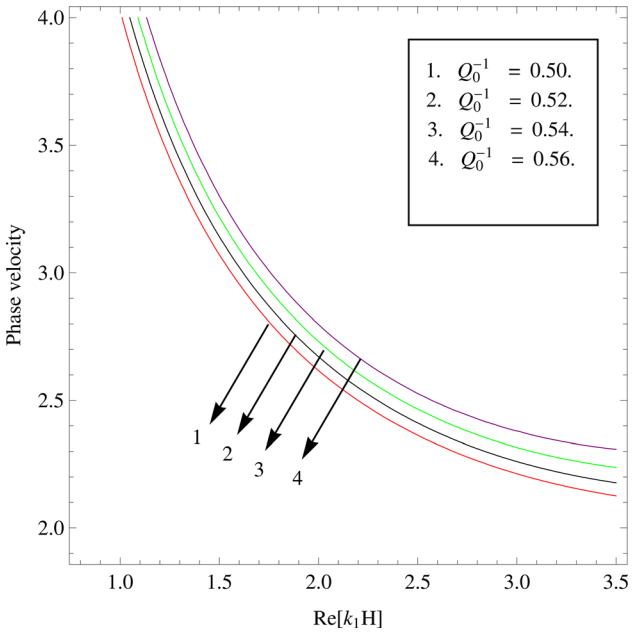

Figure 8. Variation of phase velocity against real wave number for different values of dissipation factor (Q_0^{-1}) associated with viscoelastic substrate.

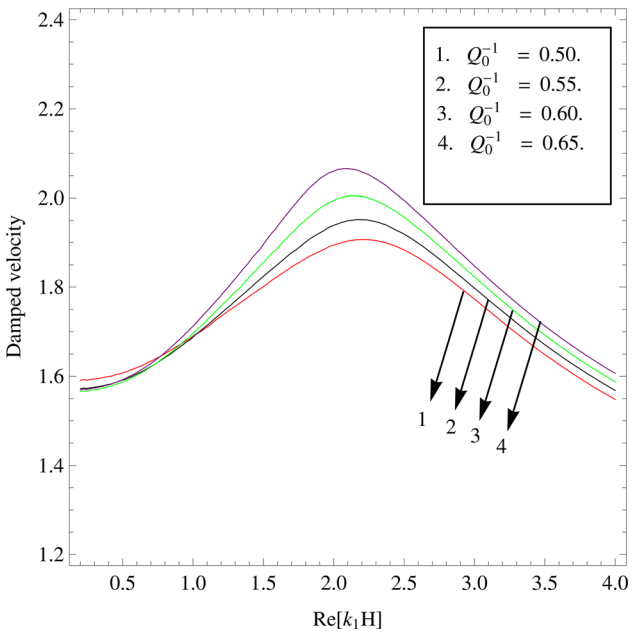

Figure 9. Variation of damped velocity against real wave number for different values of dissipation factor (Q_0^{-1}) associated with viscoelastic substrate.

The aim of figures 18 and 19 is to display the variation of phase and damped velocities under the influence of dielectric constant (T_{11}). As observed for the effect of A_{11}, here as well, the constant T_{11} has negligible influence on both the velocities. However, if closely looked upon the curves of damped velocity for both constants (A_{11} and T_{11}), it is seen that for T_{11}, the damped velocity starts at

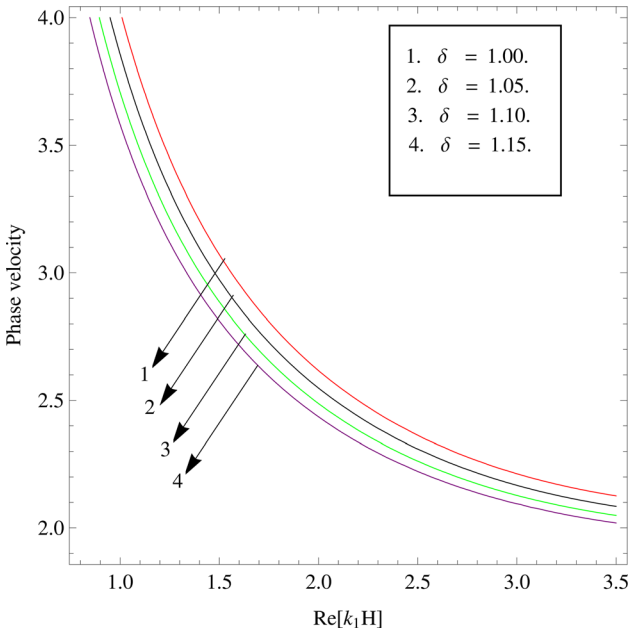

Figure 10. Variation of phase velocity against real wave number for different values of attenuation coefficient (δ).

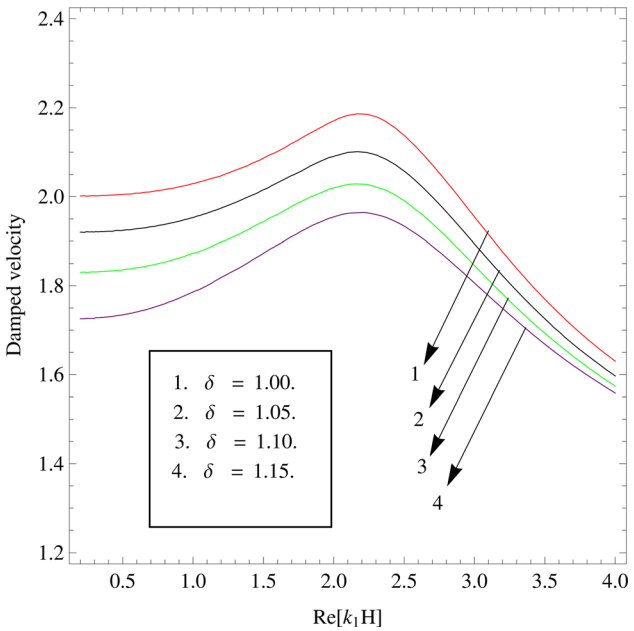

Figure 11. Variation of damped velocity against real wave number for different values of attenuation coefficient (δ).

a much higher value. It then forms a plateau-like curve which then decreases gradually afterwards.

Lastly, a general attempt has been made in figure 20 to compare the porous piezoelectric material (PPM) with the non-porous piezoelectric material. It is noticed that for PPM, there occurs a sudden decline in phase velocity with wave number. However, for a non-porous piezoelectric material, there is a small increment in phase velocity and then decreases gradually.

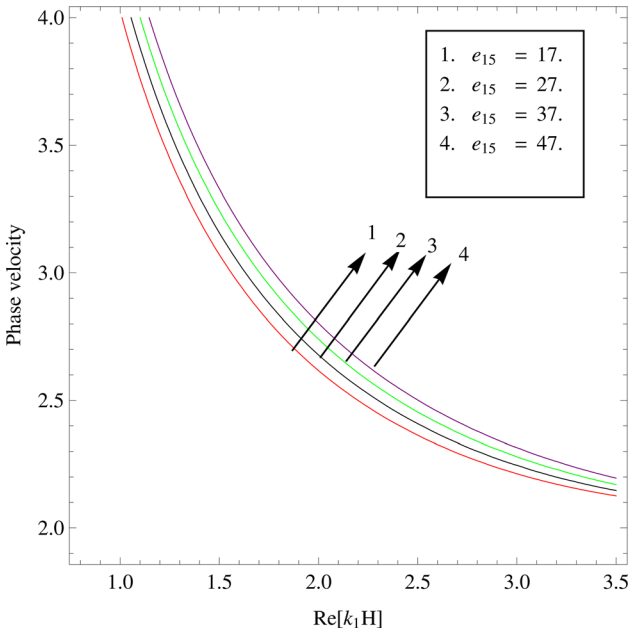

Figure 12. Variation of phase velocity against real wave number for different values of piezoelectric constant (e_{15}).

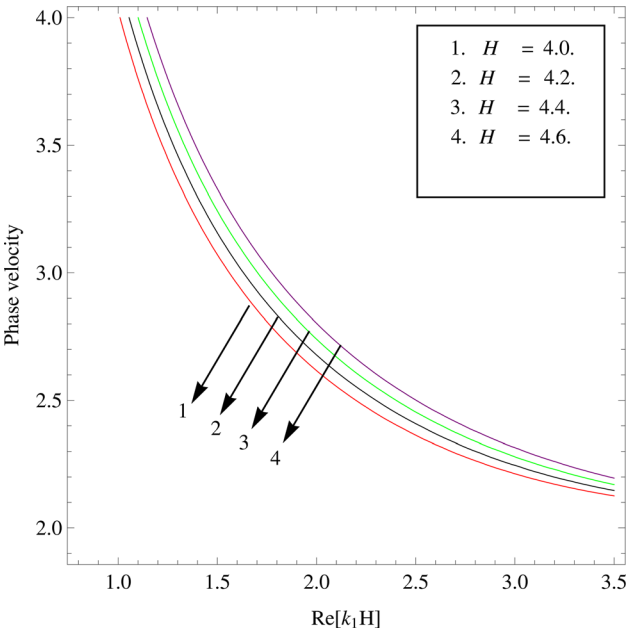

Figure 14. Variation of phase velocity against real wave number for different widths of PPM layer (H).

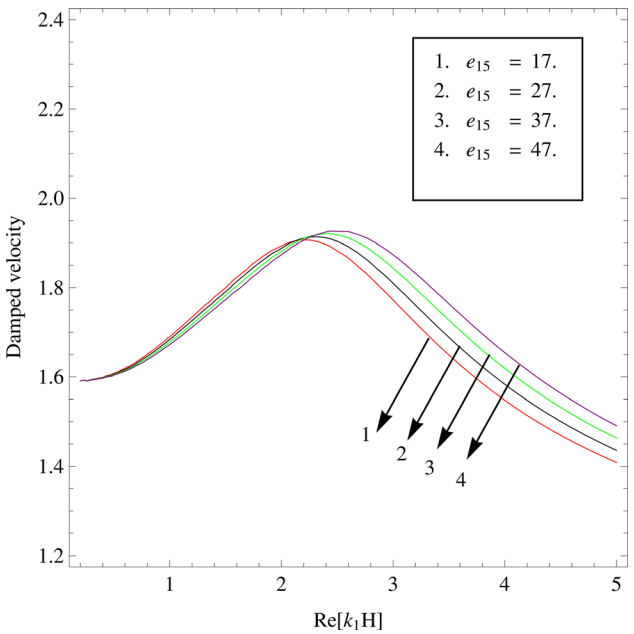

Figure 13. Variation of damped velocity against real wave number for different values of piezoelectric constant (e_{15}).

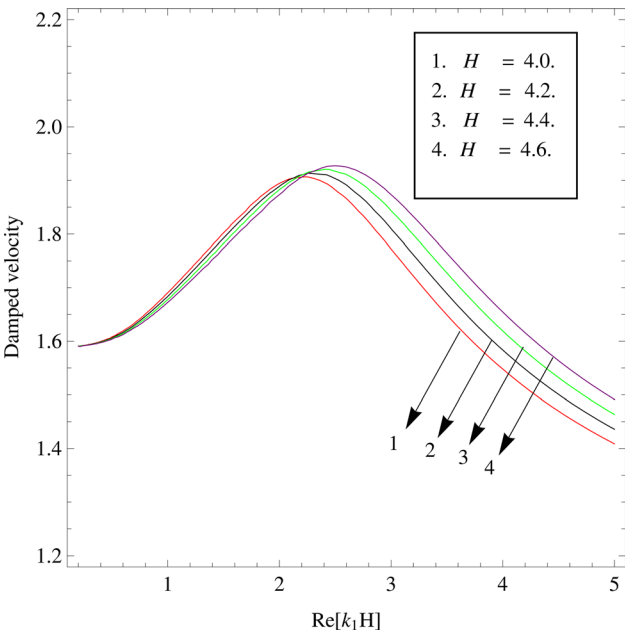

Figure 15. Variation of damped velocity against real wave number for different widths of PPM layer (H).

6. Concluding remarks

A thorough and complete analysis has been done to study the behaviour of SH-type wave in a porous piezoelectric material (PPM) layer resting over a heterogeneous viscoelastic substrate influenced by a point source. The calculation technique implemented here is Green's function technique. The variation of phase and damped velocities of SH-type wave under the influence of parameters such as heterogeneity parameter associated with rigidity, associated with internal friction and associated with density, dissipation factor, attenuation coefficient, piezoelectric constant, width of the PPM layer and dielectric constants have been studied. Here are some of the conclusive points of the analysis:

1. Closed-form solutions of frequency equation have been obtained using Green's function technique.

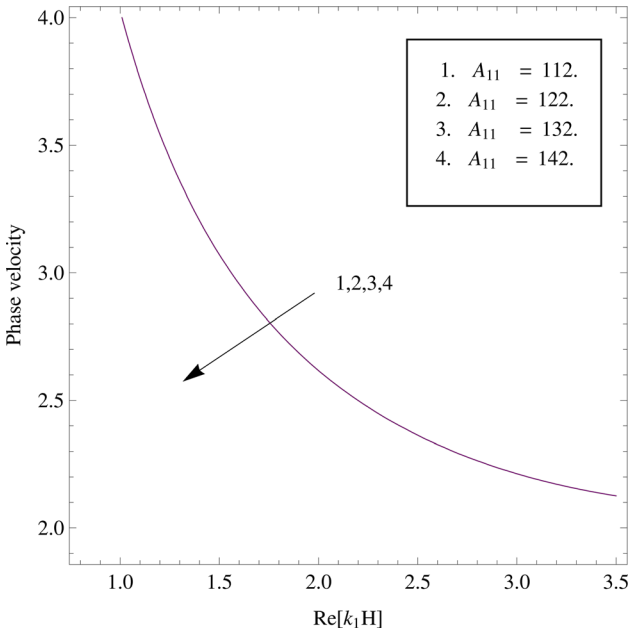

Figure 16. Variation of phase velocity against real wave number for different values of dielectric constant (A_{11}).

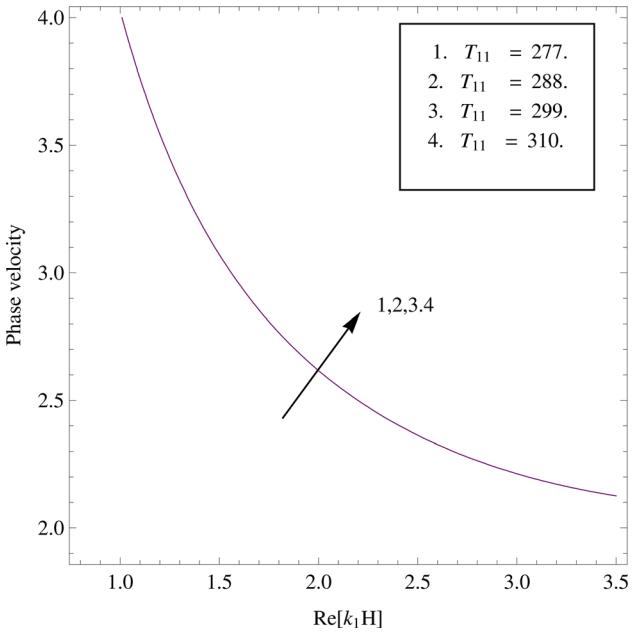

Figure 18. Variation of phase velocity against real wave number for different values of dielectric constant (T_{11}).

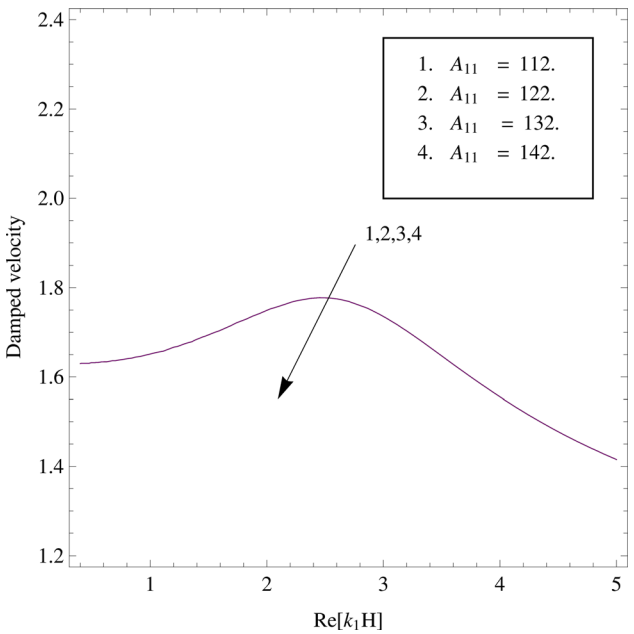

Figure 17. Variation of damped velocity against real wave number for different values of dielectric constant (A_{11}).

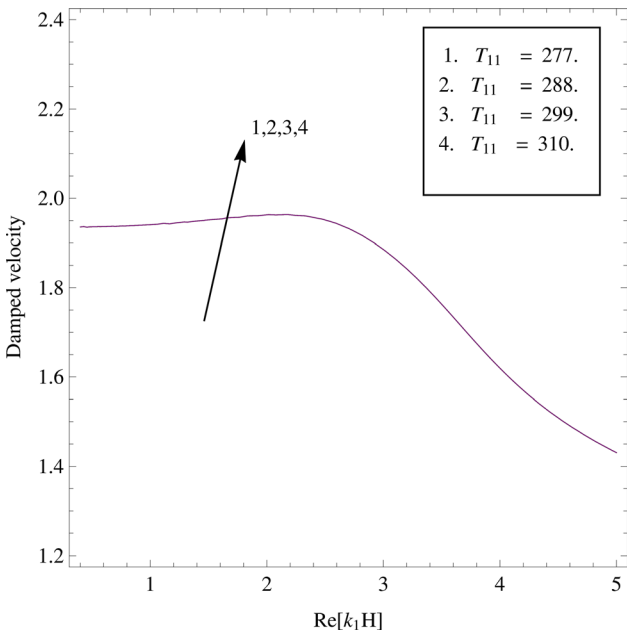

Figure 19. Variation of damped velocity against real wave number for different values of dielectric constant (T_{11}).

2. Greater the amplitude of heterogeneity associated with rigidity in the lower viscoelastic half-space, the greater the phase velocity but lower damped velocity. The phase and damped velocities are influenced more by heterogeneity associated with rigidity at the lower end of wave number.
3. The heterogeneity associated with internal friction shows mixed characteristics on the phase and damped velocities.
4. The heterogeneity associated with density and dissipation factor help in increment of both phase and damped velocities, i.e., both the velocities rise with the increase in value of the considered parameter.
5. The attenuation coefficient of the viscoelastic half-space reduces the phase and damped velocities of SH wave. The influence of this coefficient on damped velocity is predominantly more when the real wave number is small.

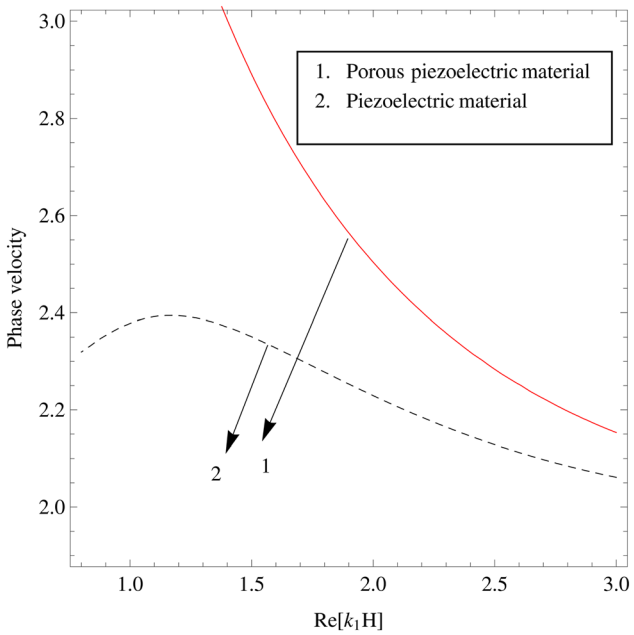

Figure 20. Comparison of real phase velocity between a porous piezoelectric material and piezoelectric materials.

6. It is established that with increasing piezoelectric constant and width, the phase velocity gets amplified. On the other hand, damped velocity does not have much influence during lower real wave numbers. But, after a certain wave number such as 2.2 approx, the peizoelectric constant and the width have a considerable influence on damped velocity.
7. The dielectric constants (A_{11} and T_{11}) have negligible influence on both the phase and damped velocities. The behaviour of phase and damped velocities remain the same irrespective of dielectric constants.
8. General outcome observed was that the phase velocity of SH-type wave was more in a porous piezoelectric material than the piezoelectric material.

As the development of any material and device is a never-ending process, therefore the current research paper has the potential to inject some useful insight into those developments. These developments can be valuable for materials used in ultrasonic imaging devices which can be extremely helpful in the medical sciences.

Acknowledgements

The authors convey their sincere thanks to DST-SERB for funding research project no. DST-SERB/2018-2019/599/AM entitled 'Analytical modelling of surface waves in fibre-reinforced and micro-polar media'.

Author statement

Neelima Bhengra: Conceptualization, exploration, methodology, software, writing – original draft, resources and formal analysis. Raju Kumhar: Methodology and resources; S Gupta: Supervision and validation. Santimoy Kundu: Supervision and validation.

Appendix A

$$t_{01} = (1-\delta)^2,\ t_{02} = 2\delta,\ b_1 = \left(\frac{\rho^p \omega^{*2}}{\overline{F}_{44}} - k_1^2\right),$$

$$t_{03} = \sqrt{\frac{\sqrt{t_{01}^2 + t_{02}^2} + t_{01}}{2}},\ t_{04} = \sqrt{\frac{\sqrt{t_{01}^2 + t_{02}^2} - t_{01}}{2}},$$

$$t_1 = \left(\frac{\rho^p \omega^{*2}}{\overline{F}_{44}} - k_1^2\right)^{1/2} t_{03},$$

$$t_2 = \left(\frac{\rho^p \omega^{*2}}{\overline{F}_{44}} - k_1^2\right)^{1/2} t_{04},$$

$$t_{05} = \frac{\left(1 - \delta Q_0^{-1}\right)}{\left(1 - \delta Q_0^{-1}\right)^2 + \left(Q_0^{-1}\right)^2},$$

$$t_{06} = \frac{Q_0^{-1}}{\left(1 - \delta Q_0^{-1}\right)^2 + \left(Q_0^{-1}\right)^2},$$

$$t_{07} = \left[\left(1 - \frac{c^2}{\beta_2^2} t_{05}\right)\left(1 - \delta^2\right) - 2\delta \frac{c^2}{\beta_2^2} t_{06}\right]$$

$$t_{08} = \left[\frac{c^2}{\beta_2^2} t_{06}\left(1 - \delta^2\right) + 2\delta\left(1 - \frac{c^2}{\beta_2^2} t_{05}\right)\right]$$

$$t_{09} = \sqrt{\frac{\sqrt{t_{07}^2 + t_{08}^2} + t_{07}}{2}},\ t_{10} = \sqrt{\frac{\sqrt{t_{07}^2 + t_{08}^2} - t_{07}}{2}},$$

$$t_{11} = k_1^n \left(t_{09}^2 + t_{10}^2\right)^{n/2} \cos\left[n \arctan\left(\frac{t_{10}}{t_{09}}\right)\right],$$

$$t_{12} = k_1^n \left(t_{09}^2 + t_{10}^2\right)^{n/2} \sin\left[n \arctan\left(\frac{t_{10}}{t_{09}}\right)\right],$$

$$\zeta_1 = \left[t_{09}\left(1 - \delta Q_0^{-1}\right) - t_{10} Q_0^{-1}\right],$$

$$\zeta_2 = \left[t_{10}\left(1 - \delta Q_0^{-1}\right) + t_{09} Q_0^{-1}\right],$$

$$\zeta_3 = [t_{07}(\chi_1 - \delta\omega^*\chi_2) - \omega^*\chi_2 t_{08} + \left((\chi_1 - \delta\omega^*\chi_2) - \chi_3 c^2\right)(1-\delta) - 2\delta\omega^*\chi_2],$$

$$\zeta_4 = [t_{08}(\chi_1 - \delta\omega^*\chi_2) - \omega^*\chi_2 t_{07} + \omega^*\chi_2(1-\delta) + 2\delta\left((\chi_1 - \delta\omega^*\chi_2) - \chi_3 c^2\right)],$$

$$\zeta_5 = [t_{07}(t_{11}t_{09} - t_{10}t_{12}) - t_{08}(t_{09}t_{12} + t_{10}t_{11})],$$

$$\zeta_6 = [t_{07}(t_{09}t_{12} + t_{10}t_{11}) + t_{08}(t_{11}t_{09} - t_{10}t_{12})],$$

$$S = \frac{\Gamma[n+1]}{2^{(n+1)} k_1}$$

$$q_1 = \mu_0 k_1(\zeta_1\zeta_5 - \zeta_2\zeta_6) + S\zeta_3,$$
$$q_2 = \mu_0 k_1(\zeta_2\zeta_5 + \zeta_1\zeta_6) + S\zeta_4,$$
$$q_3 = b_1^{1/2} F_{44}(t_{03}\zeta_5 - t_{04}\zeta_6),$$
$$q_4 = b_1^{1/2} F_{44}(t_{04}\zeta_5 + t_{03}\zeta_6).$$

Appendix B

$$t_{01} = (1-\delta)^2,\ t_{02} = 2\delta,\ b_1 = \left(\frac{\rho^p \omega^{*2}}{F_{44}} - k_1^2\right),$$

$$t_{03} = \sqrt{\frac{\sqrt{t_{01}^2 + t_{02}^2} + t_{01}}{2}},\ t_{04} = \sqrt{\frac{\sqrt{t_{01}^2 + t_{02}^2} - t_{01}}{2}},$$

$$t_1 = \left(\frac{\rho^p \omega^{*2}}{F_{44}} - k_1^2\right)^{1/2} t_{03},$$

$$t_2 = \left(\frac{\rho^p \omega^{*2}}{F_{44}} - k_1^2\right)^{1/2} t_{04},$$

$$t_{05} = \frac{\left(1 - \delta Q_0^{-1}\right)}{\left(1 - \delta Q_0^{-1}\right)^2 + \left(Q_0^{-1}\right)^2},$$

$$t_{06} = \frac{Q_0^{-1}}{\left(1 - \delta Q_0^{-1}\right)^2 + \left(Q_0^{-1}\right)^2},$$

$$t_{07} = \left[\left(1 - \frac{c^2}{\beta_2^2} t_{05}\right)\left(1 - \delta^2\right) - 2\delta \frac{c^2}{\beta_2^2} t_{06}\right]$$

$$t_{08} = \left[\frac{c^2}{\beta_2^2} t_{06}\left(1 - \delta^2\right) + 2\delta\left(1 - \frac{c^2}{\beta_2^2} t_{05}\right)\right]$$

$$t_{09} = \sqrt{\frac{\sqrt{t_{07}^2 + t_{08}^2} + t_{07}}{2}},\ t_{10} = \sqrt{\frac{\sqrt{t_{07}^2 + t_{08}^2} - t_{07}}{2}},$$

$$t_{11} = k_1^n \left(t_{09}^2 + t_{10}^2\right)^{n/2} \cos\left[n \arctan\left(\frac{t_{10}}{t_{09}}\right)\right],$$

$$t_{12} = k_1^n \left(t_{09}^2 + t_{10}^2\right)^{n/2} \sin\left[n \arctan\left(\frac{t_{10}}{t_{09}}\right)\right],$$

$$\zeta_1 = \left[t_{09}\left(1 - \delta Q_0^{-1}\right) - t_{10} Q_0^{-1}\right],$$

$$\zeta_2 = \left[t_{10}\left(1 - \delta Q_0^{-1}\right) + t_{09} Q_0^{-1}\right],$$

$$\zeta_3 = [t_{07}(\chi_1 - \delta\omega^*\chi_2) - \omega^*\chi_2 t_{08} + \left((\chi_1 - \delta\omega^*\chi_2) - \chi_3 c^2\right)(1-\delta) - 2\delta\omega^*\chi_2],$$

$$\zeta_4 = [t_{08}(\chi_1 - \delta\omega^*\chi_2) - \omega^*\chi_2 t_{07} + \omega^*\chi_2(1-\delta) + 2\delta\left((\chi_1 - \delta\omega^*\chi_2) - \chi_3 c^2\right)],$$

$$\zeta_5 = [t_{07}(t_{11}t_{09} - t_{10}t_{12}) - t_{08}(t_{09}t_{12} + t_{10}t_{11})],$$

$$\zeta_6 = [t_{07}(t_{09}t_{12} + t_{10}t_{11}) + t_{08}(t_{11}t_{09} - t_{10}t_{12})],$$

$$S = \frac{\Gamma[n+1]}{2^{(n+1)} k_1}$$

$$q_{11} = \mu_0 k_1(\zeta_1\zeta_5 - \zeta_2\zeta_6) + S\zeta_3,$$
$$q_{12} = \mu_0 k_1(\zeta_2\zeta_5 + \zeta_1\zeta_6) + S\zeta_4,$$
$$q_{13} = b_1^{1/2} F_{44}(t_{03}\zeta_5 - t_{04}\zeta_6),$$
$$q_{14} = b_1^{1/2} F_{44}(t_{04}\zeta_5 + t_{03}\zeta_6).$$

References

Aki K and Richards P G 1980 *Quantitative seismology: Theory and methods*; Freeman, San Francisco.

Arai T, Ayusawa K, Sato H, Miyata T and Kobayashi K K 1991 Properties of hydrophone with porous piezoelectric ceramics; *Japanese J. Appl. Phys.* **30**(**9S**) 253, http://iopscience.iop.org/1347-4065/30/9S/2253.

Ben-Menahem A and Singh S J 1981 Representation of seismic sources; In: *Seismic waves sources*, Springer, New York, NY, pp. 151–256.

Borcherdt R D 2009 *Viscoelastic waves in layered media*; Cambridge University Press, Cambridge.

Chan H L W, Ng P K L and Choy C L 1999 Effect of poling procedure on the properties of lead zirconate titanate/

vinylidene fluoride-trifluoro ethylene composites; *Appl. Phys. Lett.* **74**(**20**) 3029–3031, https://doi.org/10.1063/1.124054.

Chattopadhyay A, Gupta S, Kumari P and Sharma V K 2012 Effect of point source and heterogeneity on the propagation of SH-waves in a viscoelastic layer over a viscoelastic half-space; *Acta Geophys.* **60**(**1**) 119–139, https://doi.org/10.2478/s11600-011-0059-4.

Covert E E 1958 A note on an approximate calculation of Green's functions for built-up bodies; *Stud. Appl. Math.* **37**(**1–4**) 58–65, https://doi.org/10.1002/sapm195837158.

Ebrahimi F and Barati M R 2017 Damping vibration analysis of smart piezoelectric polymeric nanoplates on viscoelastic substrate based on nonlocal strain gradient theory; *Smart Mater. Struct.* **26**(**6**) 065018, http://iopscience.iop.org/0964-1726/26/6/065018.

Ebrahimi F and Dabbagh A 2017 Wave propagation analysis of smart rotating porous heterogeneous piezo-electric nanobeams; *Eur. Phys. J. Plus* **132**(**4**) 153, https://doi.org/10.1140/epjp/i2017-11366-3.

Ebrahimi F, Jafari A and Barati M R 2017 Vibration analysis of magneto-electro-elastic heterogeneous porous material plates resting on elastic foundations; *Thin Wall Struct.* **119** 33–46, https://doi.org/10.1016/j.tws.2017.04.002.

Ewing W M, Jardetzky W S, Press F and Beiser A 1957 Elastic waves in layered media; *Phys. Today* **10**(**12**) 27.

Ezzin H, Amor M B and Ghozlen M H B 2016 Love waves propagation in a transversely isotropic piezoelectric layer on a piezomagnetic half-space; *Ultrasonics* **69** 83–89, https://doi.org/10.1016/j.ultras.2016.03.006.

Ezzin H, Amor M B and Ghozlen M H B 2017 Propagation behavior of SH waves in layered piezoelectric/piezomagnetic plates; *Acta Mech.* **228**(**3**) 1071–1081, https://doi.org/10.1007/s00707-016-1744-9.

Ghosh M L 1963 On Love waves across the ocean; *Geophys. J. Int.* **7**(**3**) 350–360, https://doi.org/10.1111/j.1365-246X.1963.tb05556.x.

Gubbins D 1990 *Seismology and plate tectonics*; Cambridge University Press, Cambridge.

Gupta R K and Venkatesh T A 2006 Electromechanical response of porous piezoelectric materials; *Acta Mater.* **54** 4063–4078.

Hayashi T, Sugihara S and Okazaki K 1991 Processing of porous 3-3 PZT ceramics using capsule-free O_2-HIP; *Japanese J. Appl. Phys.* **30**(**9S**) 2243, http://iopscience.iop.org/1347-4065/30/9S/2243.

Huang S, Chang J, Lu L, Liu F, Ye Z and Cheng X 2006 Preparation and polarization of 0–3 cement-based piezoelectric composites; *Mat. Res. Bull.* **41**(**2**) 291–297, https://doi.org/10.1016/j.materresbull.2005.08.026.

Karmakar S, Sahu S A and Nirwal S 2020 Method of Green's Function for characterization of SH waves in Porous-Piezo composite structure with a point source; *J. Solid Mech.* **12**(**1**) 72–89.

Kudimova A, Mikhayluts I, Nadolin D, Nasedkin A, Nasedkina A, Oganesyan P and Soloviev A 2017 Computer design of porous and ceramic piezocomposites in the finite element package ACELAN; *Procedia Structural Integrity* **6** 301–308, https://doi.org/10.1016/j.prostr.2017.11.046.

Kumari R and Singh A K 2021 Dispersion and attenuation of shear wave in couple stress stratum due to point source; *J. Vib. Cont.* **28**(**13–14**), https://doi.org/10.1177/1077546321998880.

Kumari P, Sharma V K and Modi C 2016 Modeling of magnetoelastic shear waves due to point source in a viscoelastic crustal layer over an inhomogeneous viscoelastic half space; *Waves Random Complex Media* **26**(**2**) 101–120.

Kundu S, Kumhar R, Maity M and Gupta S 2020 Influence of point source on love-type waves in anisotropic layer overlying viscoelastic FGM half-space: Green's function approach; *Int. J. Geomech.* **20**(**1**) 04019141.

Mahanty M, Kumar P, Singh A K and Chattopadhyay A 2021 Green's function analysis of shear wave propagation in heterogeneous poroelastic sandwiched layer influenced by an impulsive source; *Wave Motion* **107** 102821.

Mizumura K, Kurihara Y, Ohashi H, Kumamoto S K and Okuno K O 1991 Porous piezoelectric ceramic transducer; *Japanese J. Appl. Phys.* **30**(**9S**) 2271, http://iopscience.iop.org/1478-7814/19/1/360.

Nasedkin A, Nasedkina A and Rybyanets A 2017 Finite element simulation of effective properties of microporous piezoceramic material with metallized pore surfaces; *Ferroelectrics* **508**(**1**) 100–107, https://doi.org/10.1080/00150193.2017.1289569.

Piazza D, Capiani C and Galassi C 2005 Piezoceramic material with anisotropic graded porosity; *J. Eur. Ceramic Soc.* **25**(**12**) 3075–3078, https://doi.org/10.1016/j.jeurceramsoc.2005.03.193.

Qian Z H, Jin F, Lu T, Kishimoto K and Hirose S 2010 Effect of initial stress on Love waves in a piezoelectric structure carrying a functionally graded material layer; *Ultrasonics* **50**(**1**) 84–90.

Saroj P K, Sahu S A, Chaudhary S and Chattopadhyay A 2015 Love-type waves in functionally graded piezoelectric material (FGPM) sandwiched between initially stressed layer and elastic substrate; *Waves Random Complex Media* **25**(**4**) 608–627, https://doi.org/10.1080/17455030.2015.1063738.

Singh A K, Das A, Mistri K C and Chattopadhyay A 2017 Green's function approach to study the propagation of SH wave in piezoelectric layer influenced by a point source; *Math. Methods Appl. Sci.* **40**(**13**) 4771–4784, https://doi.org/10.1002/mma.4343.

Singh A K, Das A, Ray A and Chattopadhyay A 2018 On point source influencing Love-type wave propagation in a functionally graded piezoelectric composite structure: A Green's function approach; *J. Intell. Mater. Syst. Struct.*, https://doi.org/10.1177/1045389X18754351.

Singhal A, Sahu S A and Chaudhary S 2018a Approximation of surface wave frequency in piezo-composite structure; *Compos. B: Eng.* **144** 19–28, https://doi.org/10.1016/j.compositesb.2018.01.017.

Singhal A, Sahu S A and Chaudhary S 2018b Liouville-Green approximation: An analytical approach to study the elastic waves vibrations in composite structure of piezo material; *Compos. Struct.* **184** 714–727, https://doi.org/10.1016/j.compstruct.2017.10.031.

Taunaumang H, Guy I L and Chan H L W 1994 Electromechanical properties of 13 piezoelectric ceramic/piezoelectric polymer composites; *J. Appl. Phys.* **76**(**1**) 484–489, https://doi.org/10.1063/1.357099.

Vashishth A K, Dahiya A and Gupta V 2015 Generalized Bleustein–Gulyaev type waves in layered porous piezoceramic structure; *Appl. Math. Mech.* **36**(**9**) 1223–1242.

Wang Q, Chen Q, Zhu J, Huang C, Darvell B W and Chen Z 2008 Effects of pore shape and porosity on the properties of porous LNKN ceramics as bone substitute; *Mater. Chem. Phys.* **109**(**2–3**) 488–491, https://doi.org/10.1016/j.matchemphys.2007.12.022.

Xia Z, Ma S, Qiu X, Wu Y and Wang F 2003 Influence of porosity on the stability of charge and piezoelectricity for porous polytetrafluoroethylene film electrets; *J. Electrostat.* **59**(**1**) 57–69, https://doi.org/10.1016/S0304-3886(03)00089-5.

Zeng T, Dong X, Mao C, Chen S and Chen H 2006 Preparation and properties of porous PMN–PZT ceramics doped with strontium; *Mat. Sci. Eng.*: *B* **135**(**1**) 50–54, https://doi.org/10.1016/j.mseb.2006.08.039.

Corresponding editor: Munukutla Radhakrishna